EARLY RESULTS FROM AN IMAGING INTERFEROMETER PROTOTYPE OPERATING IN THE SAGNAC CONFIGURATION

Paolo Marcoionni*,[a]

*Parma University – Earth Sciences Department, Parco Area delle Scienze 157A, 43100 Parma, ITALY
[a]National Research Council – "Nello Carrara" Applied Physics Institute, via Panciatichi 64, 50147 Firenze, ITALY
P.Marcoionni@ifac.cnr.it

Submit to: YOUNG FORUM SESSIONS on Remote Sensing

KEYWORDS: Imaging interferometer, hyperspectral remote sensing, calibration methods, image processing.

ABSTRACT

Recent advances in Earth remote sensing imagers have being attempted with the launch of the first Fourier Transform Hyperspectral Imager placed on board of U.S. Department of Defence. From the analysis of alternative optical layouts for a stationary interferometer, we have developed a laboratory imaging interferometer operating in the Sagnac configuration. This instrument does not employ any moving part to optically scan the instrument field-of-view, and acquires the image of the observed target modulated from a staring interference pattern of vertical fringes. Despite of traditional Michelson-like interferometers, the intensity autocorrelation functions are generated by moving the concerned scene with respect to the imaging device. In this paper we present some laboratory measurements obtained by this new stationary imaging interferometer. In order to calibrate the instrument response and to determine its spectral resolution, we have executed a set of measurements illuminating a planar double diffuser with a red He-Ne laser. The dependence of the optical-path-differences on the source spectral content has been assessed observing a 600W halogen lamp with interference filters having 10nm of bandwidth. In order to retrieve at-sensor radiance spectrum a calibration procedure of the acquired data has been implemented, which also takes into account dark signal subtraction, instrument spatial response compensation, geometrical and radiation distortion correction, DC-offset subtraction, and inverse cosine transform. Some hints are given about the use of such an instrument on board of airborne platforms for remote sensing of the Earth.

1. INTRODUCTION

The launch of the first Fourier Transform Hyperspectral Imager (FTHSI) on board of U.S. Air Force Research Laboratory technological satellite MightySat II.1 has been an attempt to overcome the main drawbacks that limit the use of push-broom and whisk-broom imaging spectrometers for Earth remote sensing applications (Otten et al, 1998; Otten et al, 1995).
The FTHSI optical concept is derived from the so-called "stationary imaging interferometers" which don't use any moving part to optically scan the instrument Field-Of-View (FOV). In the FTHSI instrument the complete interferogram of the light from a slit is obtained by means of a cylindrical lens which spatially disperses the physical information on one axis of the employed detector array. Movement of the satellite with respect to the target allows the instrument to scan all the observed surface.
Differently from more conventional time-scanning instruments, in a stationary interferometer the range of Optical Path Difference (OPD) between the recombined beams generated by amplitude splitting, is obtained as a pattern of stationary fringes of "equal thickness" onto the detector array plane (Geneste et al, 1998).
System precursors of FTHSI have been the HyperCam and the IrCam developed by the Kestrel Corporation (USA) for airborne applications, the Spatially Modulated Fourier Transform Spectrometer (SMIFTS) developed by Hawaii University (Lucey et al, 1992), the High Èndue Imaging Fourier Transform Spectrometer (HEIFTS) by Science Application International Corporation (USA) (Horton, 1996), and the imaging interferometer developed by Applied Spectral Imaging (Israel) for laboratory microscopy applications (Cabib, 1996).
Many advantages arise from using these systems regarding high optical efficiency (Jacquinot and Felgett effects) and the circumstance that the detectable spectral range and resolution can be changed by acting on the sensor sampling step and the instrument FOV (Descour, 1997; Herring et al, 1993; Junttila et al, 1991).
From a radiometric point of view this circumstance provides a significant improvement of the signal-to-noise ratio (SNR). However, due to the nature of the acquired interferogram it is necessary to employ detectors with high accuracy of digitalization (Junttila, 1991).
Other critical points are connected with the high data-rate requested and the need to spectrally pre-filter the incoming radiation in order to avoid aliasing artefacts in the retrieved spectrum (Bracewell, 1965; Goodman, 1968).
Starting from the analysis of FTHSI optical configuration, a laboratory prototype imaging interferometer operating in the Sagnac configuration has been developed.
In Section two the instrument concept is presented and Section three is devoted to physical background. The description of the experimental activities we have performed in order to calibrate the instrument response is depicted in Section four. In Section five some preliminary results are presented and discussed and in Section six open problems and conclusion are drawn.

2. OPTICAL CONFIGURATION

The typical layout of the developed instrument, called Sagnac configuration, is shown in Figure 1.

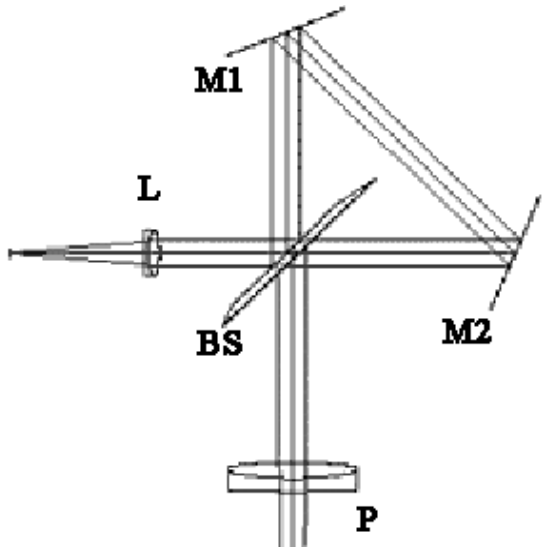

Figure 1. Conceptual layout of the stationary interferometer arranged in the Sagnac (triangular or cyclic path) geometry

The light from the object is first collimated by the objective L, and, by means of a beam-splitter BS and two folding mirrors M1 and M2, is focused onto a CCD plane by the lens P. Like the Michelson device, this Sagnac interferometer also uses a beam-splitter (as source-doubling technique) but inside of a common (triangular) path with a tilt introduced between the two interfering image wavefronts to form a fixed (stationary) pattern of interference fringes of "equal thickness".

The BS is the fundamental component, which provides phase-delay between the two coherent interfering rays so that the OPD changes linearly with varying the angle of the entering ray with respect to the instrument optical axis. Therefore, the device acquires the image of an object superimposed to a fixed pattern of across-track interference fringes. Then, introducing a relative motion between the sensor and the object, each scene pitch experiences the same interference pattern and an entire image-frame is recorded for each autocorrelation phase offset.

The 3-D array of these frames has to be "realigned" in order to extract the complete autocorrelation function (interferogram) of each scene pixel, then this record is inverse cosine transformed to yield a wavenumber hyperspectral data cube.

Differently from the FTHSI optical configuration, our prototype interferometer doesn't employ the slit nor the cylindrical lens in front of the detector array. In fact, in the developed version a complete 2-D image of the observed scene is acquired with superimposed the autocorrelation modulation pattern.

The main feature is that we need acquire as many frames as the number of photosensitive elements. For example, if we utilize a detector array with 512 pixels, it is necessary to acquire a set of 512 records to reconstruct the complete autocorrelation function of each scene pixel. It is clear that the requested data-rate is very high.

Figure 2 shows a picture of the developed instrument.

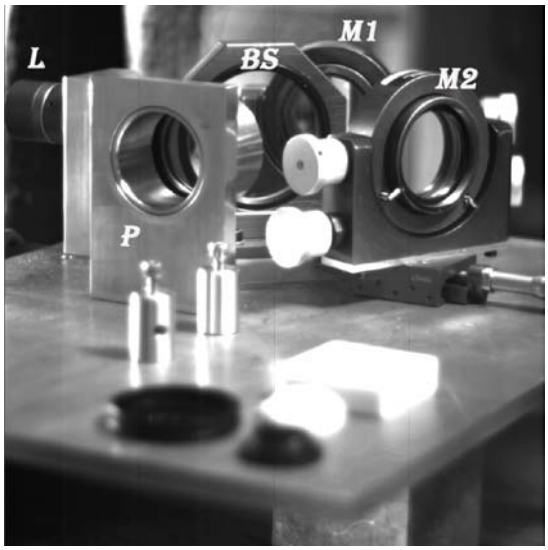

Figure 2. Picture of the developed instrument

The characteristics of the CCD camera used to spatially resolve the interferogram are listed in Table 3.

Type:	CCD frame-transfer with anti-blooming, TH7888A
Number of pixel:	1024 x 1024
Pixel size	14 µm x 14 µm
Spectral range:	430 nm-1000 nm @QE>3%
Responsivity:	23DN/(nJ cm^2) @450 nm 18% @680 nm
Dynamic range:	3200:1
Maximum frame/rate:	60 fps
Digitalization:	12 bit

Table 3. Characteristics of the frame grabber used to spatially resolve the interferogram record

In our case, the data cube of a typical measurement contains more than 1 million data points for a total size of 2 MB before cosine transform.

3. PHYSICAL BACKGORUND

In a Fourier Transform Spectrometer (FTS) the acquired physical information is the interferogram $I(OPD)$, which depends on OPD values according to the following fundamental law (Barnes, 1985; Okamoto et al, 1984):

$$I(OPD) = \int \frac{I_0(k)}{2}\left[1+\cos(2\pi k OPD)\right]dk \qquad (1)$$

where $I_0(k)$ is the intensity of the ray entering the interferometer, OPD is the optical path difference introduced by the BS in the considered propagation direction, $k = 1/\lambda$ is the wavenumber and the integration takes into account for a non-monochromatic light spectrum.

For $OPD = 0$ the interferogram reaches its maximum value at each wavelength, this property being assured by the circumstance that the phase delay between a certain pair of interfering ray is generated inside the semi-transparent plate.
The complete raw interferogram of the energy coming from a certain pixel of the observed scene is not a continuous function of OPD but it is convolved by the pixel dimension p, and sampled with a square grid (the sampling step is considered equal to the pixel dimension) whose extension is limited by the detector size D. Therefore, in the X space of pixel coordinates the measured interferogram $\overline{I(x)}$ may be expressed as:

$$\overline{I(x)} \approx \left[I(OPD(x)) * rect(\frac{x}{p}) \right] comb(\frac{x}{p}) rect(\frac{x}{D}) \qquad (2)$$

It can be easily shown that the relationship between OPD and the entering ray direction ϑ with respect to the instrument optical axis is linear, as long as the device FOV is not superior to a few degrees, as stated by:

$$OPD(\vartheta) \approx a\vartheta \approx \frac{a}{f} x \qquad (3)$$

being a the constant, which expresses the direct proportionality between OPD and ϑ, and f the effective focal length of the lens focusing the interference image. The constant a is related to the maximum digitised optical path difference $OPD_{\max}$ and to the maximum angle $\vartheta_{\max}$.
The raw interferogram is constituted by a pair of values $(x, DN(x))$, which indicate respectively the pixel position on the matrix and the corresponding electronic signal expressed in digital number.
The spatial coordinate x of a certain pixel is related to the sampling step p we have assumed to be identical to the pixel dimension, being j the integer index of the considered sample and j_0 the position corresponding to null OPD. From previous relationships, Eq.3 can be rewritten as:

$$OPD(\vartheta) = \frac{a}{f}(j - j_0)p \qquad (4)$$

The inverse cosine transformed interferogram $\overline{\overline{I(k)}}$ is:

$$\overline{\overline{I(k)}} \approx \left[I(k)\mathrm{sinc}(\delta OPDk) \right] * comb(\delta OPDk) * \mathrm{sinc}(2OPD_{\max}k) \qquad (5)$$

where δOPD is the optical path difference subtended by two adjacent pixels of the detector array.
This relationship yields an important limit for the sampling frequency to avoid aliasing in the retrieved spectrum $I(k)$. As stated by Shannon's theorem the chosen sampling frequency k_s should be grater than the bandwidth $k_{\max}$ of the concerned signal. In our case it should occur that:

$$k_s = \frac{1}{2\delta OPD} \geq k_{\max} \qquad (6)$$

From Eq.6 results that the minimum wavelength $\lambda_{\min}$ we can reconstruct without any effects of spectral aliasing is $\lambda_{\min} = 2\delta OPD$. Obviously another limit on this quantity is dictated by the detector sensitivity.

4. INTERFEROGRAM MEASUREMENT

In order to calibrate in wavenumber (or in OPD) the interferometer response and to determine its spectral resolution, an experimental activity has been carried out in our laboratory.
A double planar diffuser has been illuminated with a He-Ne laser ($\lambda_{laser} = 632.8nm$, output power~20mW) to obtain a spatially coherent homogeneous and isotropic radiation field at the interferometer entrance.
This experimental set-up allowed us to get a complete interferogram from a single image, strongly reducing the measurements time and the experiment complexity.
In Figure 4 a single frame obtained with the laser source is shown.

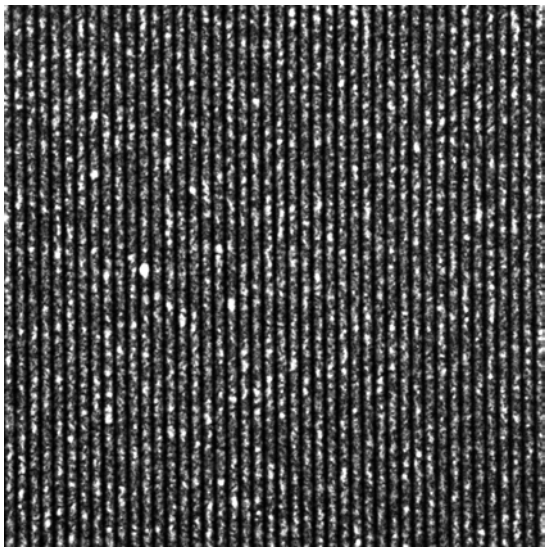

Figure 4. Raw image (in gray scale) obtained illuminating a double planar diffuser with a red He-Ne laser. The image is filled with a pattern of across-track interference fringes of "equal thickness".

As can be seen, the interference fringes are vertical lines which completely fill the image-frame and the high number of these stripes is due to the high intrinsic coherence-degree of the employed radiation source. In our case this number is, in practice, limited by the maximum angular divergence of the entering rays.
A 600W halogen lamp has also been used with the aforementioned double diffuser. The result is shown in Figure 5.

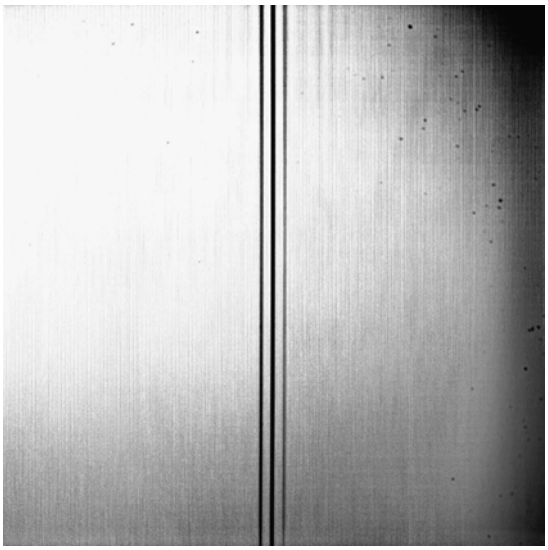

Figure 5. Raw image (in gray scale) obtained illuminating a double planar diffuser with a 600W halogen lamp.

As can be seen, the number of interference fringes is smaller than in the previous image due to the broad spectral content of the radiation source. Moreover, the strong central fringe which corresponds to null interference is black, i.e. for the rays coming along the instrument optical axis their phase-delay is π .
In Figure 6 the same lamp has been seen trough an interferential filter with bandwidth of 10 nm centered at 640 nm.

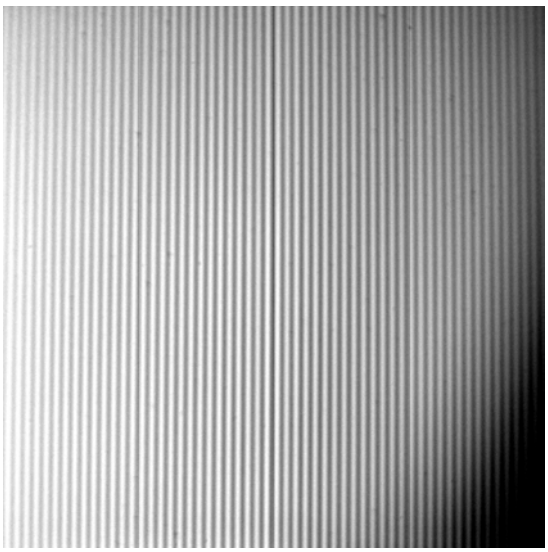

Figure 6. Raw image (in gray scale) obtained illuminating a double planar diffuser with a 600W halogen lamp seen through an interferential filter centered at 640 nm and wide 10 nm.

Reducing the spectral content of the radiation source by filtering, the interferogram becomes more similar to that produced by a "quasi-monochromatic" signal. It is also evident the effect of vignetting on the acquired frame.

5. RETRIEVED SPECTRA

From the frames depicted in Figure 4 and Figure 6, it has been extracted the corresponding interferogram averaged over all image pixels.

Since the acquired image is produced from a spatially coherent uniform radiation source, the interferogram extracted from each horizontal line is, with good approximation, equal to the interferogram of the energy from a fixed pixel. In a different wording, it is not necessary to acquire a complete set of frames (data-cube) to reconstruct the full interferogram of the concerned pixel.
In Figure 7 and Figure 8 the average interferograms have been plotted.

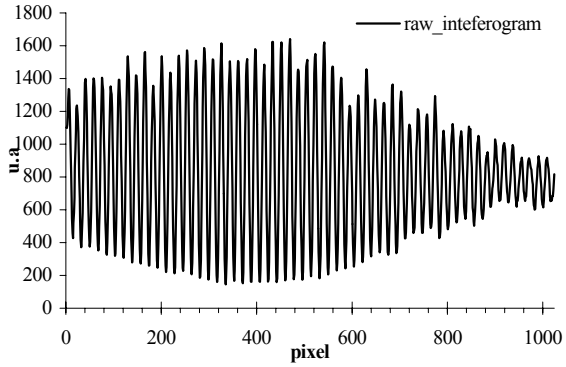

Figure 7. Interferogram averaged over all the columns of image of Figure 4.

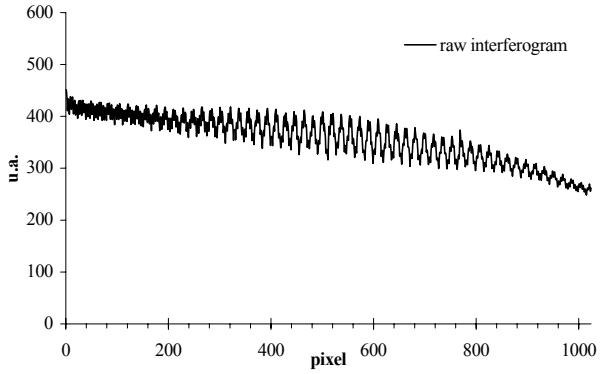

Figure 8. Interferogram average over all the columns of image of Figure 6.

The pre-processed interferogram should have a null-mean, starting and ending tails approaching to zero, and any optical artefact removed. In order to achieve these characteristics, we have pre-processed our data according to the following scheme (Barducci and Pippi, 2001):

1) dark signal subtraction (to account for bias and noise in the detector electronic stage);
2) instrument spatial response compensation (to remove saturated pixels, hot and cold pixels, and fixed-pattern noise);
3) geometrical and radiometric distortion correction (to remove effects of vignetting and spatial shift of the fringes);
4) DC-offset subtraction to estimate the band-averaged energy reaching the detector as expressed by the term $I_0(k)/2$ in (1);

5) apodization to avoid "Gibbs effect" (ringing);
6) inverse cosine transform application to retrieve at-sensor radiance spectrum.

An ideal interferogram, therefore, is symmetric with respect to the zero path difference and contains cosine contributions only. However, a misaligned sampling grid, which doesn't match the region of zero path difference, results in an evident asymmetry in a real interferogram profile as it happens in Figures 7-8.
The spectrum of the employed laser source has been retrieved (result of inverse cosine transform), and is plotted in Figure 9, where we have not adopted any apodization technique.

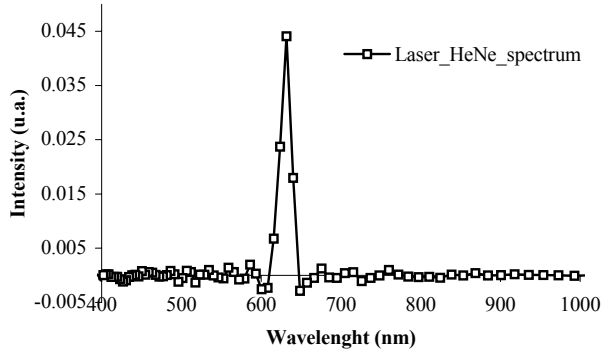

Figure 9. Uncalibrated spectrum of radiance retrieved from the interferogram depicted in Figure 7.

As already stated this type of interferometer needs neither a slit nor an aperture, leading to much larger flux of light available than that from traditional dispersive spectrometer. However, the resolving power of this system $R = k_{\max} / \delta k$ is determined only by the number N of photosensitive elements of the detector array. This is the main reason that has led us to employ a 1024-elements array.
Moreover, for a continuous spectrum, most of the radiation energy is concentrated in the central fringes of the interferogram but the physical information more relevant is distributed on the wings of the interferogram. Therefore, the detector needs a large dynamic range, which, in turns, determines the maximum variability of signal over the image.
The spectral resolution seems to take great advantage from this experimental set-up. Due to the circumstance that the employed spectral source may be approximated to an impulse-like radiation field, the measurement above described is also a good test to estimate the instrument spectral resolution δk , which obeys the following law (Persky, 1995):

$$\delta k = \frac{1}{2OPD_{\max}} \qquad (7)$$

The obtained spectral resolution is about 175 cm^{-1} (which corresponds to 7 nm at 632 nm) across the entire bandwidth. According to (4) the related maximum optical path difference is about 30 μm.
However, we believe this result could be improved because spectral resolution has been lost due to two main troubles which affected the shown data. The first one concerns with the circumstance that the Nyquist cut-off frequency of the input spectrum as filtered from the detector spectral sensitivity did not match the available sampling frequency, thus generating aliasing in the blue side of the spectrum. The second trouble reason is related to the adopted optical configuration. We have verified that a different distance between the two folding mirrors can improve the obtained spectral resolution.
In Figure 10 six frames of a brief sequence of measurements (images of the sky and landscape around Florence) are shown. Let us note how the scene details seem to move from left to right while the pattern of interference fringes remains fixed.

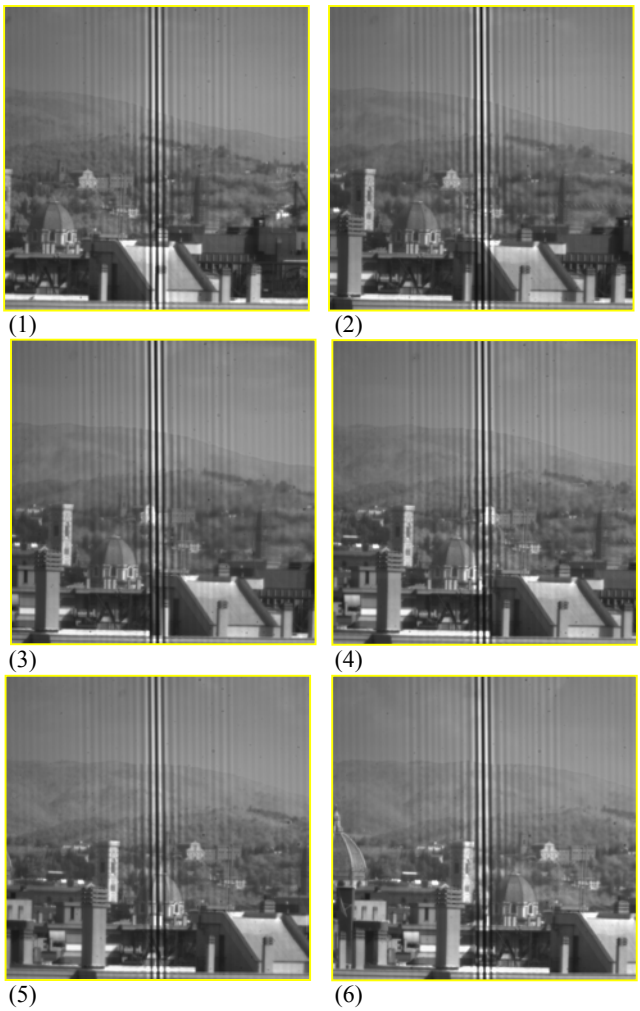

Figure 10. Six frames of a brief sequence of measurements (images of the sky and landscape around Florence city).

As can be seen, the number of interference fringes is smaller than that obtained in previous laboratory measurements due to the poor coherence degree of the solar radiation.
Data processing is currently under evaluation in order to retrieve physical properties from these images.

6. CONCLUDING REMARKS

In this paper a new stationary imaging interferometer operating in the Sagnac configuration (developed at our laboratory) has been discussed. Experimental activity has been carried out in order to calibrate the instrument response and to measure its spectral resolution. Some problems connected to data processing methodology have been discussed regarding in particular dark-signal removal, DC offset compensation, inverse cosine transform routine implementation, and noise filtering.

Finally, the option to improve radiometric and spectral performance by acting on the optical configuration has been analyzed in the prospective to employ the developed instrument on board of an airborne platform for Earth remote sensing purposes.

7. REFERENCES

Barducci, A., Pippi, I., 2001. Analysis and rejection of systematic disturbances in hyperspectral remotely sensed images of the Earth, *Applied Optics,* 40, pp. 1464 – 1477.

Barnes, T. H., 1985. Photodiode array Fourier transform spectrometer with improved dynamic range. *Applied Optics*, 24(22), pp. 3702 – 3706.

Bracewell, R., 1965. *The Fourier transform and its applications*. McGraw-Hill, New York.

Cabib, D., Buckwald, R. A., Garin, Y., Soenksen, D. G., 1996. Spatially resolved Fourier transform spectroscopy (spectral imaging): a powerful tool for quantitative analytical microscopy. *Proceeding of SPIE – Optical diagnostics of living cells on biofluids*, Vol. 2678, pp. 278 – 291.

Descour, M. R., 1997. The Throughput Advantage In Imaging Fourier-Transform Spectrometers. In: *Proceeding of SPIE – Imaging Spectrometry II*, Vol. 2819, pp. 285 – 290.

Genest, J., Tremblay, P., and Villemaire, A., 1998. Throughput of tilted interferometers. *Applied Optics*, 37(21), pp. 4819 – 4822.

Goodman, J. W., 1968. *Introduction to Fourier Optics*. McGraw-Hill, New York.

Herring, M., Chrien, T. G., Duval, V. G., Kabrach, T. N., 1993. Imaging spectrometry: concepts and system trade-offs. In: *Proceeding of SPIE – Infrared and Millimeter-Wave Engineering*, Vol. 1874, pp. 11 – 23.

Horton, R. F., 1996. Optical Design for High Ètendue Imaging Fourier Transform Spectrometer. In: *Proceeding of SPIE - Imaging Spectrometry II*, Vol. 2819, pp. 300 – 315.

Junttila, M. -L., 1992. Stationary Fourier transform spectrometer. *Applied Optics*, 31, pp. 4106 – 4112.

Junttila, M. -L., Kauppinen, J., and Ikonen, E., 1991. Performance limits of stationary Fourier spectrometers. *Journal of Optical Society of America A*, 8(9), pp. 1457 – 1462.

Lucey, P. G., Williams, T., Horton, K., Budney, C., Ratfer, J. B., and Risk, E. T., 1992. SMIFTS: A cryogenically cooled spatially modulate, imaging, Fourier transform spectrometer for remote sensing applications. In: *Proceeding of the International Conference on Spectral Sensing Research*, Vol. 1, pp. 251 – 262.

Okamoto, T., Kawata, S., and Minami, S., 1984. Fourier transform spectrometer with a self-scanning photodiode. *Applied Optics*, 23(2), pp. 269 – 273.

Otten, L. J., Meigs, A. D., Jones, B. A., Prinzing, P., and Fronterhouse, D. S., 1998. Payload Qualification and Optical Performance Test Results for the MightySat II.1 Hyperspectral Imager. In: *Proceeding of SPIE - Sensors, Systems, and Next Generation Satellites II*, Vol. 3498, pp. 231 – 238.

Otten, L. J., Sellar, R. G., and Rafert, J. B., 1995. MyghtySatII.1 Fourier transform hyperspectral imager payload performance. In: *Proceeding of SPIE - the Advanced and Next Generation Satellites*, Vol. 2583, pp. 566 – 575.

Persky, M. J., 1995. A review of spaceborne infrared Fourier transform spectrometers for remote sensing. *Review of Scientific Instruments*, 66(10), pp. 4763 – 4797.

8. ACKNOWLEDGEMENTS

This research is partially supported by the Italian Space Agency (ASI) under the research contract I/R/172/02. The author thanks A. Barducci for his interest on Fourier Optics and his precious reviewing of the presented work. This paper would not have possible without the contribution of I. Pippi of the "Nello Carrara" Applied Physics Institute. I gratefully acknowledge the help of F. Castagnoli, M. Morandi and D. Guzzi and for everyone else involved in making this experiment possible.